Contents lists available at ScienceDirect

Arabian Journal of Chemistry

journal homepage: www.ksu.edu.sa

Original article

Synthesis of g-C_3N_4 decorated with ZIF-8 and $CuFe_2O_4$ as a highly efficient and magnetically separable photocatalyst for degradation of tetracycline

Anjan Kumar [a], Ali M. Hussein [b], Farag M.A. Altalbawy [c], Mandeep Kaur [d,e], Harpreet Kaur [f,g], Sarah Salah Jalal [h], Salah Hassan Zain Al-Abdeen [j], Khursheed Muzammil [k], Merwa Alhadrawi [l,m,n,*]

[a] Department of electronics and communication engineering, GLA University, Mathura, India
[b] Department of Biomedical Sciences, College of Science, Cihan University-Erbil, Kurdistan Region, Iraq
[c] Department of Chemistry, University College of Duba, University of Tabuk, Tabuk, Saudi Arabia
[d] Department of Chemistry, School of Sciences, Jain (Deemed-to-be) University, Bengaluru, Karnataka 560069, India
[e] Department of Sciences, Vivekananda Global University, Jaipur, Rajasthan 303012, India
[f] School of Basic & Applied Sciences, Shobhit University, Gangoh, Uttar Pradesh 247341, India
[g] Department of Health & Allied Sciences, Arka Jain University, Jamshedpur, Jharkhand 831001, India
[h] College of Pharmacy/National University of Science and Technology, Dhi Qar, Iraq
[j] Department of Medical Laboratories Technology, AL-Nisour University College, Baghdad, Iraq
[k] Department of Public Health, College of Applied Medical Sciences, Khamis Mushait Campus, King Khalid University, Abha, Saudi Arabia
[l] Department of Refrigeration and air Conditioning Techniques, College of Technical Engineering, the Islamic University, Najaf, Iraq
[m] Department of Refrigeration and air Conditioning Techniques, College of Technical Engineering, the Islamic University of Al Diwaniyah, Al Diwaniyah, Iraq
[n] Department of Refrigeration and air Conditioning Techniques, College of Technical Engineering, the Islamic University of Babylon, Babylon, Iraq

ARTICLE INFO

Keywords:
Photocatalyst
ZIF-8/g-C_3N_4/$CuFe_2O_4$ nanocomposite
Tetracycline
Wastewater treatment

ABSTRACT

In this study, for the first time a magnetically recoverable zeolitic imidazolate framework-8 (ZIF-8) / graphite carbon nitride (g-C_3N_4)/ cooper ferrite ($CuFe_2O_4$) nanocomposite was prepared through a fast and simple wet impregnation procedure. The magnetic behavior of the ZIF-8/g-C_3N_4/$CuFe_2O_4$ heterostructure was used for the easy recovery of the nanocomposite by an external magnet. After studying the structural, crystallinity, magnetic, and photophysical properties of the as-syntesized sample, its application was investigated for the enhanced photodegradation of tetracycline under visible light illumination. The band gap energies for ZIF-8, g-C_3N_4, and $CuFe_2O_4$ were obtained 5.1 eV, 2.8 eV, and 1.3 eV, respectively. After combination of ZIF-8, g-C_3N_4, and $CuFe_2O_4$, the band gap energy was obtained to 2.4 eV, which indicate the improvement of photocatalytic activity of ZIF-8/g-C_3N_4/$CuFe_2O_4$ nanocomposite. Among the as-synthesized photocatalyst samples, the ZIF-8/g-C_3N_4/$CuFe_2O_4$ showed an excellent photocatalytic activity (99.15 %) for degradation of tetracycline within 65 min irradiation of visible light, solution pH of 5 and photocatalyst dosage of 0.75 g/L. The rate constant of the ZIF-8/g-C_3N_4/$CuFe_2O_4$ is almost 13.1, 9.9, and 15.6 times higher than that of ZIF-8, g-C_3N_4, and $CuFe_2O_4$, respectively. The ZIF-8/g-C_3N_4/$CuFe_2O_4$ heterojunction showed the effective degradation activity for four consecutive cycles, which exhibited its excellent reusability and stability. Moreover, the free radical quenching tests confirmed that holes, and hydroxyl radicals were the main reaction species for degradation of tetracycline. Altogether the preparation of novel ZIF-8/g-C_3N_4/$CuFe_2O_4$ provides an promise avenue for the development of high potential magtenticaly photocatalytic systems for sustainable tetracycline production with remarkable efficiencies.

1. Introduction

Antibiotics have been admitted as one of the potential environmental pollutants, which is a serious threat to ecological balance and human health (Zhou et al., 2023; Chin et al., 2023). Antibiotics have been applied in aquaculture, disease control, animal husbandry, agricultural production and discharged into the environment from different sources such as hospitals, sewage treatment plants, livestock breeding, and

* Corresponding author at: Department of Refrigeration and air Conditioning Techniques, College of Technical Engineering, the Islamic University, Najaf, Iraq.
E-mail address: merwaalhadrawil@gmail.com (M. Alhadrawi).

https://doi.org/10.1016/j.arabjc.2024.105912
Received 7 April 2024; Accepted 17 July 2024
Available online 20 July 2024

pharmaceutical plants agricultural land (Liu et al., 2024; Tang et al., 2024; Sun et al., 2024). Most of the antibiotics cannot be completely metabolized, so excreted by metabolites or prototypes and lead to serious environmental pollution (Davies et al., 2021; Chen et al., 2021). Especially, antibiotics lead to toxic effects such as increased drug resistance, carcinogenicity associated with their accumulation, and complexation with metals (Baaloudj et al., 2021; Wei et al., 2020). Among the antibiotics, tetracycline (TC) is one of the broad-spectrum antibiotics, which is not completely absorbed by the body and is not completely eliminated by water treatment plants (Wu et al., 2023; Liu et al., 2023). Therefore, developing efficient technologies to removal of TC has aroused prior attention (Li et al., 2023; Zhou et al., 2022; Yuan et al., 2023; Wang et al., 2021). Among various developed technologies, photocatalytic degradation has been widely applied for eliminating various organic TC (Li et al., 2021; Ding et al., 2023; Heris et al., 2023; Luo et al., 2023). Therefore, the design and development of novel and efficient photocatalysts is requisite for the removal of TC, thereby declining the harm of TC.

Recently, zeolitic imidazolate framework −8 (ZIF-8), which is a research hot pot in the removal of water contaminants, has been extensively used in photocatalytic systems due to large surface area, thermal and chemical stability, and high porosity (Ammar et al., 2023; Chen et al., 2023; Rabeie and Mahmoodi, 2023). Nevertheless, the photocatalysis capability of the ZIF-8 is limited because of various shortenings such as a large band gap (4.9–5.1 eV), weak responsivity to visible light irradiation, poor electron discharge capacity, and unwanted recombination of photo-induced electron hole pairs (Motora et al., 2023; Hong et al., 2023; Mittal et al., 2023). The main disadvantages of the ZIF-8 are dissolved using adopting different strategies, namely, heterojunction structures, doping, and co-doping (Hu et al., 2024; Xie et al., 2022; Sun et al., 2020). To date, ZIF-8 nanocomposites have been successfully fabricated with different materials such as metal oxides, polymers, graphene, carbon nanotubes (CNTs), and so on (Li et al., 2023; Qiu et al., 2023; Gowriboy et al., 2022). These nanocomposites have attracted widespread attention because they show superior properties to pure samples via the collective behavior of each single phase. Compared with individual ZIF-8, the combination of ZIF-8 with other materials increases the photodegradation performance of ZIF-8, and also broadens its application range. For instant, Li and coworkers have synthesized the ZIF-8@TiO_2 micron composite via the hydrothermal method and used as a photocatalyst for the degradation of TC (Li et al., 2020). The results showed that, the incorporation of ZIF-8 improved the photocatalytic performance of the nanocomposite compared to pure TiO_2. In another study, Zhou et al. synthesized ZIF-8-doped Cu_2O via an in situ growth method. The as-prepared nanocomposite was shown superior removal efficacy and good stability (Zhou et al., 2022).

Graphite carbon nitride (g-C_3N_4) is a metal-free organic polymer semiconductor that has aroused growing interest in the field of water pollutant removal due to its outstanding properties like nontoxicity, low cost, facile synthesis, good stability, and visible-light absorption bandgap (2.73 eV) (Khan et al., 2023; Palanivel et al., 2019; El Messaoudi et al., 2023; Ranjithkumar et al., 2021). g-C_3N_4 can be easily synthesized with a wide variety of procedures such as chemical vapor deposition (Urakami et al., 2023), thermal polymerization (Song et al., 2024), and solvothermal (Hu et al., 2017) in the various forms of nanosheets, nanoparticles, nanotubes, and so on. However, the practical applications of g-C_3N_4 have been limited by two main factors including fast electron-hole recombination and low surface area (Pattanayak et al., 2023; Hayat et al., 2023). These drawbacks can be overcome via material design strategies such as morphological control, doping, surface modification, defect engineering, and especially via the formation of nanocomposites (da Silva et al., 2023). For example, g-C_3N_4/TiO_2 heterojunction was prepared by Zhang and co-workers, and it can be degrade about 99.04 % tetracycline within 120 min (Zhang et al., 2022). It is expected that the formation of g-C_3N_4/ZIF-8 nanocomposite leads to overcoming the disadvantages of each of them.

In recent years, copper- and iron-based semiconductors have great application potential in the photocatalysis field due to their economy, and low toxicity. Among these materials, $CuFe_2O_4$ is an efficient photocatalyst due to good visible light response, stable structure, and unique magnetic properties which assist the recycling of photocatalysts (Truong et al., 2023; Rouibah et al., 2023). However, pure $CuFe_2O_4$ exhibits low photocatalytic activity, due to a narrow band gap and fast recombination rate of photoinduced charges, and as a result, only a small amount of charge carriers participate in the degradation reaction (Ramadevi et al., 2023; Cai et al., 2021). On the other hand, the combination of $CuFe_2O_4$ with other semiconductors is known to show excellent photodegradation performance under visible light illumination. In 2022, CuO/$CuFe_2O_4$/g-C_3N_4 was synthesized by Lei's group, and degraded about 99 % tetracycline under simulated sunlight (Li et al., 2022).

There are various methods to address the limitations of semiconductors such as ZIF-8, g-C_3N_4, and $CuFe_2O_4$. Among these methods, the formation of heterojunction structures has

has received much attention (Yue et al., 2024; Zhao et al., 2023; Zhao et al., 2023; Zhao et al., 2023).To the best of our knowledge, the ternary ZIF-8/g-C_3N_4/$CuFe_2O_4$ photocatalyst has not been reported for the removal of TC. ZIF-8, g-C_3N_4, and $CuFe_2O_4$ are some of the most promising materials for the removal of water pollutants via photocatalytic degradation. Therefore, it is expected that the combination of these three semiconductors and construction of nanocomposite lead to improved photocatalytic activity compared to their bare phases. In the present study, the novel magnetic ZIF-8/g-C_3N_4/$CuFe_2O_4$ nanocomposite was prepared via wet impregnation procedure and after characterization was used for photocatalytic degradation of TC under visible light irradiation. Moreover, incorporation of ZIF-8 and $CuFe_2O_4$ into g-C_3N_4 further enhanced the removal efficiency of TC.

2. Experimental details

2.1. Materials and characterization

Iron (III) nitrate nonahydrate ($Fe(NO_3)_3{\cdot}9H_2O$), zinc nitrate hexahydrate ($Zn(NO_3)_2{\cdot}6H_2O$, 99 %), copper nitrate trihydrate ($Cu(NO_3)_2{\cdot}3H_2O$), 2-methylimidazole (99 %), Methanol (MeOH, 99.5 %), Melamine, and sodium hydroxide (NaOH), were purchased from Sigma Aldrich or Merck companies and used without any further purification.

Phase identification of as-synthesized samples was analyzed on Bruker d8 Advance Diffractometer. FT-IR analysis was performed on a Nicolet Avatar 370 spectrometer. MIRA3 TESCAN field emission scanning electron microscopy (FESEM) equipped with an.

energy dispersive X-ray spectrometer (EDS) instrument was applied for microstructural, and elemental characterization. Transmission electron microscopy (TEM) analyses were carried out on a G2F20S-TWI (Tecnai, American) at 200 kV. The magnetic properties of the as-synthesized samples were investigated on a VSM, 7400, Lakeshare. UV–visible absorption spectra and diffuse reflectance spectra (DRS) of the as-synthesized samples were obtained by Shimadzu UV-2550PC UV–Vis Spectrophotometer. Zetasizer Nano-ZS was used to measure the zeta potential of samples. Photoluminescence (PL) test was performed on a LS55 spectrofluorometer. Electrochemical impedance spectroscopy (EIS) were assessed by an electrochemical analyzer (Zahner PP211). The amount of leached Fe and Cu elements was studied by an atomic absorption spectrophotometer (AAS, Perkin Elmer 900S). The total organic carbon (TOC) data were collected by a Shimadzu, TOC-Vcph analyzer. Bruker A300 was used for electron spin resonance (ESR) measurements of samples using 2,2,6,6-Tetramethylpiperidine oxide (TEMPO), and 5,5-dimethyl-1-pyrroline oxide (DMPO) under visible light and dark.

2.2. Preparation of ZIF-8

ZIF-8 was synthesized via ultrasound-assisted method. For this

purpose, 1.25 mmol of $Zn(NO_3)_2{\cdot}6H_2O$ and 10 mmol of 2-methylimidazole were added to 15 mL methanol separately. In the next step, the solution of 2-methylimidazole was slowly added to the zinc nitrate solution and ultrasonicated for 2 h. Then, the product was centrifuged and washed five times with methanol. Finally, the white precipitation was dried in a vacuum oven at 60 °C for 12 h.

2.3. Preparation of g-C_3N_4

In a typical synthesis, a certain amount of melamine was put into a muffle furnace and heated to 550 °C for 4 h. Then, for the preparation of g-C_3N_4 nanosheets, the yellow product was grounded to powder, dispersed in methanol, and ultrasonicated for 2 h. The precipitate was collected with centrifugation and washed several times with distilled H_2O. Finally, the yellow sample was dried at 70 °C in an oven.

2.4. Preparation of $CuFe_2O_4$

First, 5 mmol $Fe(NO_3)_3{\cdot}9H_2O$, and 2.5 mmol $Cu(NO_3)_2{\cdot}3H_2O$ were added to 100 mL distilled water and magnetically stirred. Subsequently, NaOH solution (4 M) was slowly added into the solution and magnetically stirred for 1 h. The resultant mixture was maintained in an oven at 90 °C for 2 h. The dark brown magnetic product was separated with an external magnet. Finally, the sample was washed several times by distilled H_2O and dried in an oven at 70 °C.

2.5. ZIF-8/g-C_3N_4/$CuFe_2O_4$ nanocomposite

The ZIF-8/g-C_3N_4/$CuFe_2O_4$ nanocomposite was fabricated via an ultrasonic-assisted wet impregnation procedure. A certain amount of g-C_3N_4 (50 wt%) was added into a 50 mL ethanol/water mixture (1:1) ratio and ultrasonicated for 1 h. Then certain amounts of ZIF-8 (30 wt%) and $CuFe_2O_4$ (20 wt%) were added to the above solution and stirred for 24 h. Finally, the obtained nanocomposite was centrifuged and dried at 70 °C.

2.6. Photocatalytic activity test

Typically, a certain amount of as-synthesized photocatalyst was added into 100 mL TC solution of the selected concentration. After 30 min of stirring in the dark (300 rpm), the suspension had been exposed to visible light for a specific time, coming from 50 W LED lamps ($\lambda >$ 420 nm). After every 15 min of reaction, 1.5 mL of suspension was withdrawn, and exposed to the magnetic field at once and the liquid lying above was moved into a quartz cell to measure the residual concentration of TC using the UV–vis spectrophotometer at λ_{max} = 365 nm (Shimadzu UV-2550PC UV–Vis Spectrophotometer, Japan). The optimization of the parameters for the photodegradation of TC using ZIF-8/g-C_3N_4/$CuFe_2O_4$ nanocomposite was carried out using catalyst loadings in the range of 0.45–0.75 g/L, TC concentrations in the range of 15–45 ppm, initial solution pH values in the range of 3–9. The efficiency of TC degradation (%D) was calculated by the formula of (%D) = (A_0-A) / A_0 × 100, where A_0 is the absorbance intensity of TC solution before irradiation and A indicate the absorbance intensity of TC after irradiation for a certain time (Govindan et al., 2017; Govindan et al., 2013).

3. Results and discussion

3.1. Characterization of photocatalyst

The crystallinity of the samples was studied by XRD analysis. As exhibited in Fig. 1A, the XRD pattern of pure ZIF-8 is well matched with the other samples reported in the literature. For this sample, the diffraction peaks at 2θ = 7.37°, 10.40°, 12.73°, 14.69°, 16.45°, 18.03°, 22.12°, 24.49° and 26.65° are related to (011), (002), (112), (022), (013), (222), (114), (233) and (134) planes, respectively. These

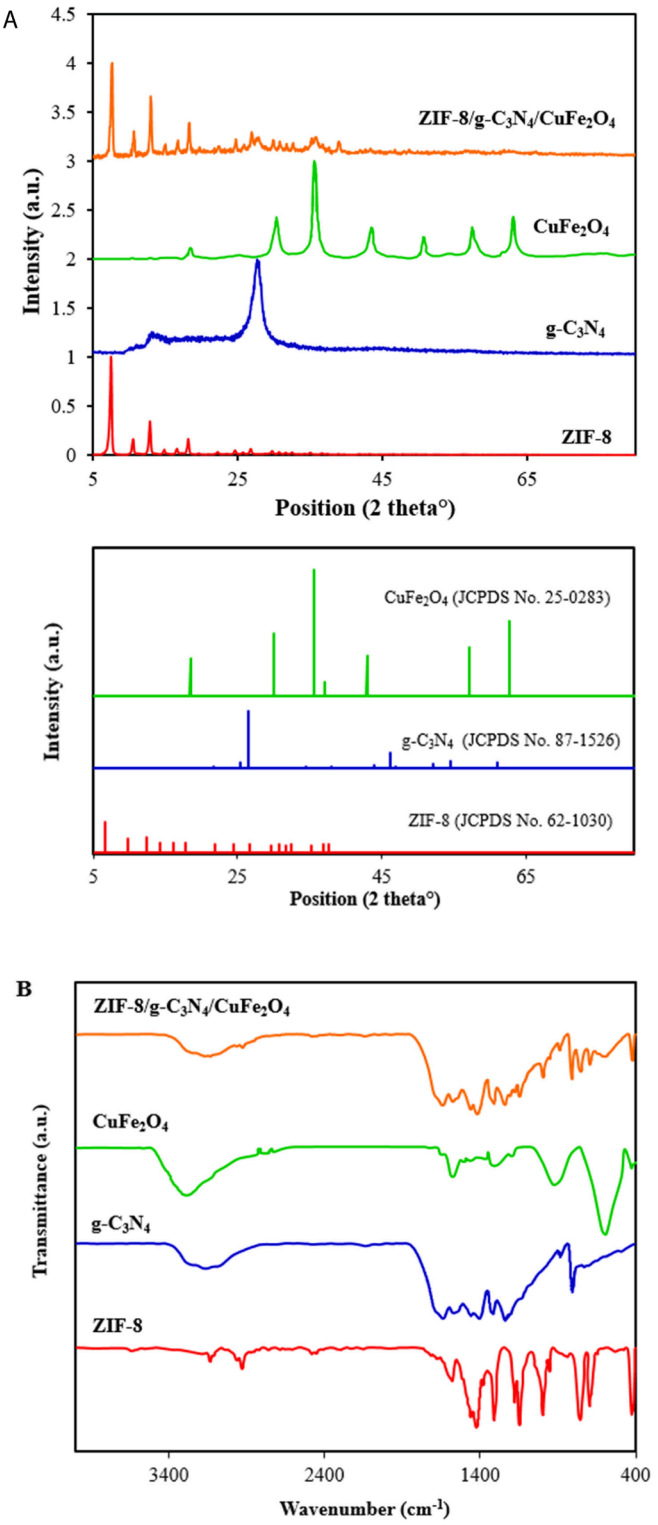

Fig. 1. XRD patterns (A), and FTIR spectra (B) of ZIF-8, $CuFe_2O_4$, g-C_3N_4, and ZIF-8/g-C_3N_4/$CuFe_2O_4$ nanocomposite.

reflections are in accordance with the sodalite (SOD)-type structure of ZIF-8 (JCPDS No. 62–1030). The XRD pattern of g-C_3N_4 exhibited diffraction peaks at 2θ = 13.05° and 27.70° with corresponding hkl planes of (100), and (002) plans, respectively (JCPDS No. 87–1526). For pure $CuFe_2O_4$, the characteristic diffraction peaks at 2θ = 18.52°, 30.19°, 35.78°, 43.05°, 57.02° and 62.78°, which are assigned to (111), (220), (311), (400), (511) and (440) hkl planes, respectively. Each

diffraction peak of pristine $CuFe_2O_4$ is well matched with the spinel cubic phase of $CuFe_2O_4$ (JCPDS No. 25–0283). The XRD pattern of the ZIF-8/g-C_3N_4/$CuFe_2O_4$ nanocomposite reveals that the main distinct peaks of ZIF-8, g-C_3N_4, and $CuFe_2O_4$ still coexist and no impurity diffraction peaks were observed. This confirms that ZIF-8, and $CuFe_2O_4$ have been successfully incorporated on the surface of g-C_3N_4 nanosheets.

The functional groups of the samples were examined by FT-IR analysis and the related spectra were exhibited in Fig. 1B. As presented in Fig. 1B, the absorption band at 422 cm^{-1} is corresponded to the stretching vibration of Zn-N bond which indicates that Zn was successfully linked to the nitrogen atoms of 2-methylimidazole (Wang et al., 2020). The absorption bands from 600 cm^{-1} to 1500 cm^{-1} are related to the stretching and bending vibration of the imidazole ring, and also the absorption peak at 1576 cm^{-1} is assigned to C=N bonding stretching vibration. In addition, the peaks located at 2929 cm^{-1} and 3135 cm^{-1} belonged to the aromatic ring and the aliphatic chain in 2-methylimidazole, respectively (Abdi, 2020). For pure g-C_3N_4, the peaks at 806 and 1640 cm^{-1} are assigned to s-triazine ring units and C=N stretching vibration, respectively. In addition, the peaks around 1240, 1320, 1410, and 1570 cm^{-1} are related to stretching vibration of aromatic C–N. As for $CuFe_2O_4$, two peaks at around 450 and 590 cm^{-1} are attributed to stretching vibration of metal–oxygen at the tetrahedral and octahedral sites in spinel structures, respectively. Moreover, after the combination of ZIF-8, g-C_3N_4, and $CuFe_2O_4$ and the formation of ZIF-8/g-C_3N_4/$CuFe_2O_4$ nanocomposite, the characteristic bands of ZIF-8, g-C_3N_4, and $CuFe_2O_4$ coexisted in the FT-IR spectrum of the nanocomposite, revealing the successful formation of the nanocomposite.

Imaging analysis was performed to study the morphology, and particle size of synthesized samples, by means of FE-SEM. Pure g-C_3N_4 (Fig. 2A) shows a tow dimensional nanosheet structure, confirming successful formation of g-C_3N_4 from in bulk nature. As illustrated in Fig. 2B, ZIF-8 was shown rhombohedral dodecahedron morphology with average particle sizes of around 90 nm. As can be seen in Fig. 2C, $CuFe_2O_4$ displayed a spherical shape with a uniform particle size which aggregated together. It is clear from Fig. 2D that ZIF-8 and $CuFe_2O_4$ were well dispersed on the surface of the g-C_3N_4 nanosheets, which reveals the successful corporation of ZIF-8 and $CuFe_2O_4$ on the surface of g-C_3N_4. In addition, the elemental analysis of the as-synthesized ZIF-8/g-C_3N_4/$CuFe_2O_4$ nanocomposite was examined by EDS analysis. As illustrated in Fig. 3A, six elements of Zn, N, C, Cu, Fe, and O exist in the nanocomposite.

To observe the morphology of ZIF-8/g-C_3N_4/$CuFe_2O_4$ nanocomposite more clearly, the TEM analysis was also performed. The TEM image of the ZIF-8/g-C_3N_4/$CuFe_2O_4$ in Fig. 3B shows that the rhombohedra of ZIF-8 and nanoparticles of $CuFe_2O_4$ are distributed on the surface of g-C_3N_4 nanosheet. These results was confirm the successful synthesis of ZIF-8/g-C_3N_4/$CuFe_2O_4$ nanocomposite.

The magnetic properties of $CuFe_2O_4$ and ZIF-8/g-C_3N_4/$CuFe_2O_4$ nanocomposite were evaluated by VSM analysis. Fig. 4 shows the magnetization curves of $CuFe_2O_4$ and ZIF-8/g-C_3N_4/$CuFe_2O_4$ nanocomposite. As can be seen, both the samples clearly shown ferromagnetic behavior at room temperature. The saturation magnetism of the pure $CuFe_2O_4$ (28 emu/g) is higher than that of nanocomposite (4 emu/g) owing to the fact that the non-magnetic ZIF-8, g-C_3N_4 coating declined the magnetic nature of $CuFe_2O_4$. The ZIF-8/g-C_3N_4/$CuFe_2O_4$ nanocomposite has excellent saturation magnetism and is efficiently separated from aqueous solution with an external magnetic field.

The band gap of the ZIF-8, g-C_3N_4, $CuFe_2O_4$, and ZIF-8/g-C_3N_4/$CuFe_2O_4$ nanocomposite has been specified by UV–Vis DRS analysis and the obtained results were shown in Fig. 5A. Tauc plots (Fig. 5B) were used to determine the band gap of the samples using the following

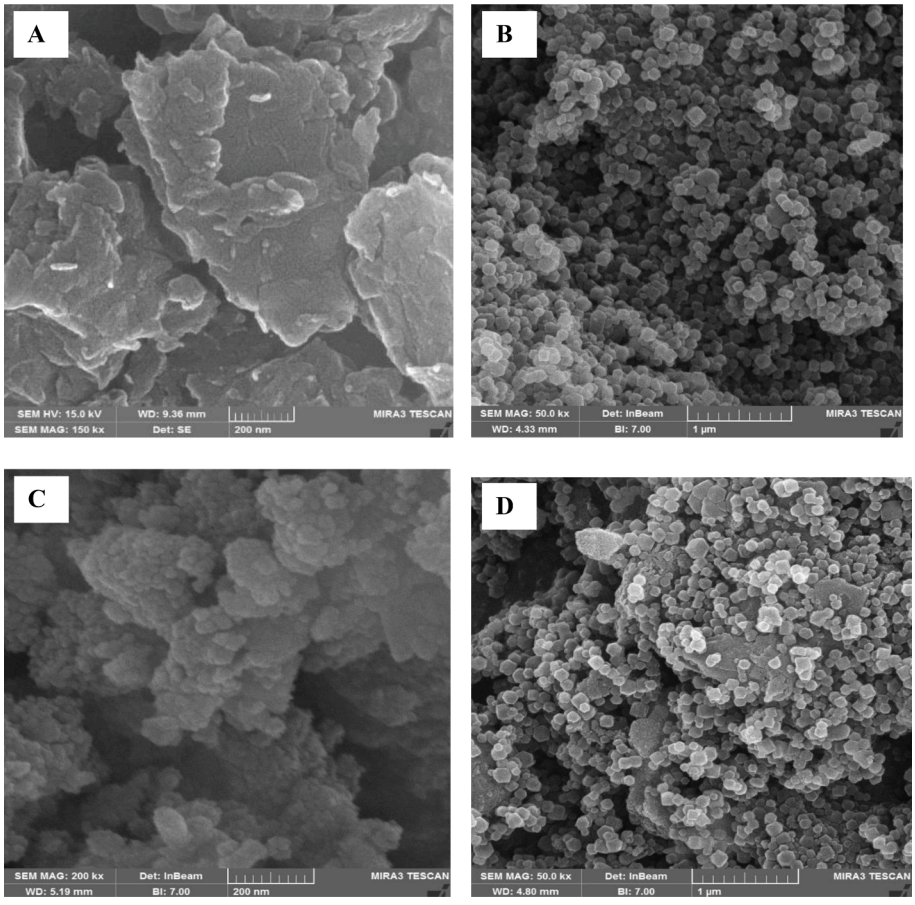

Fig. 2. FE-SEM images of g-C_3N_4 (A), ZIF-8 (B), $CuFe_2O_4$ (C), ZIF-8/g-C_3N_4/$CuFe_2O_4$ nanocomposite (D).

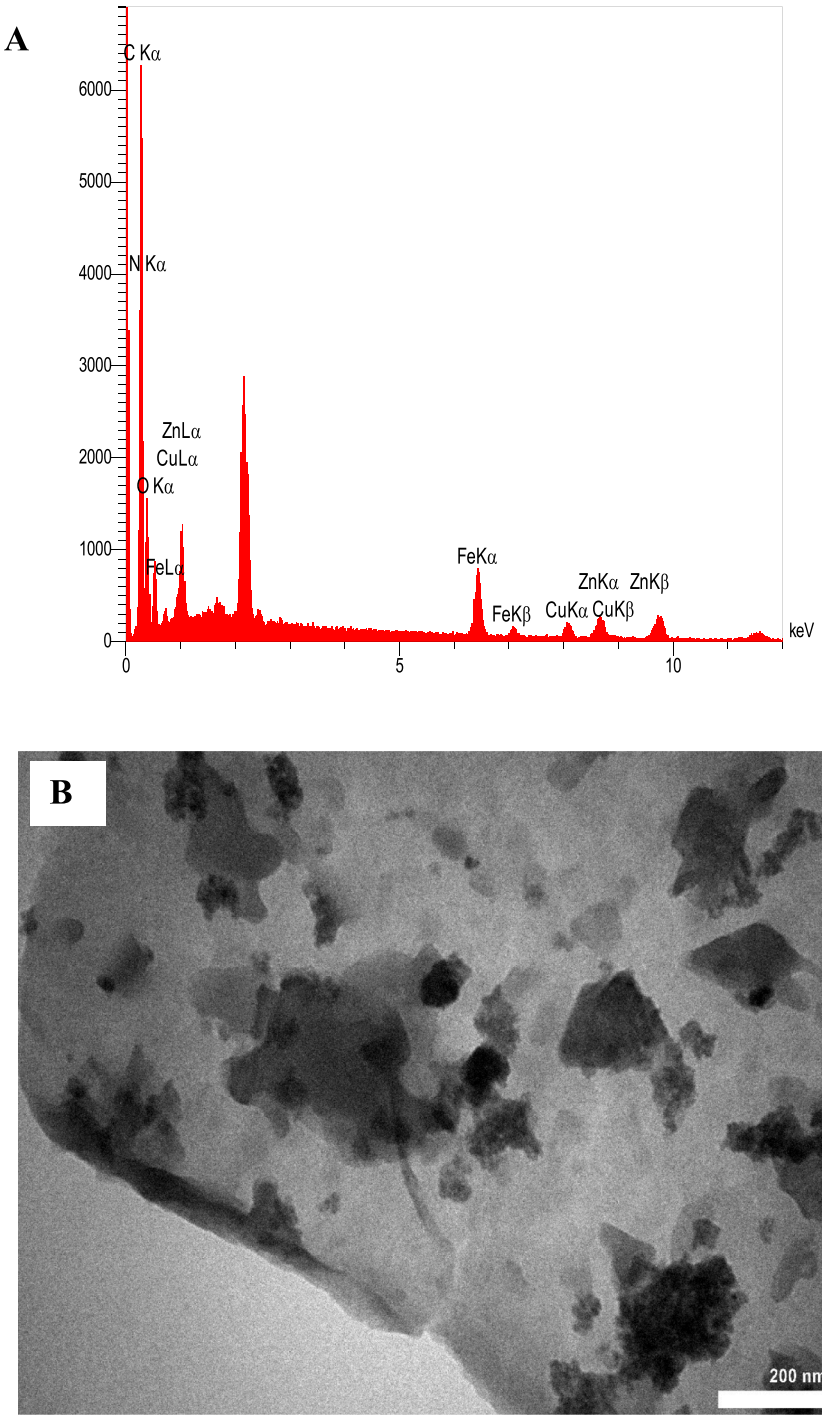

Fig. 3. EDS spectrum (A), and TEM image of ZIF-8/g-C_3N_4/$CuFe_2O_4$ nanocomposite (B).

equation:

$$(\alpha h\nu)^2 = A(h\nu - E_g)$$

Where, α and ν are the absorption coefficient and light frequency, A is a constant, and E_g indicates the band gap energy. The band gap values for ZIF-8, g-C_3N_4, $CuFe_2O_4$, and ZIF-8/g-C_3N_4/$CuFe_2O_4$ were calculated as 5.1 eV, 2.8 eV, 1.3 eV, and 2.4 eV, respectively. As a result, the construction of the heterojunction between ZIF-8, g-C_3N_4, and $CuFe_2O_4$ can enhance the absorption efficiency of visible light and also improve the production of photoexcited charge carriers and photocatalytic performance.

PL spectroscopy was used to study the migration and separation of electron-hole pairs in as-synthesized samples and the results show in Fig. 6A. As can be seen, ZIF-8 was shown the lowest PL peak intensity, indicating the lower rate of photogenerated charge carriers recombination, while $CuFe_2O_4$ and g-C_3N_4 have the high PL intensity. Furthermore, the peak intensity of ZIF-8/g-C_3N_4/$CuFe_2O_4$ is lower than that of pristine $CuFe_2O_4$ and g-C_3N_4, which signifies the coupling ZIF-8, g-C_3N_4, and $CuFe_2O_4$ inhibits recombination of photogenerated electron-hole pairs and improves the photocatalyst activity.

EIS technique was used to further study the transfer and separation of photogenerated charge carriers, and also charge transfer resistance properties of samples. EIS Nyquist plots was shown in Fig. 6B and it is

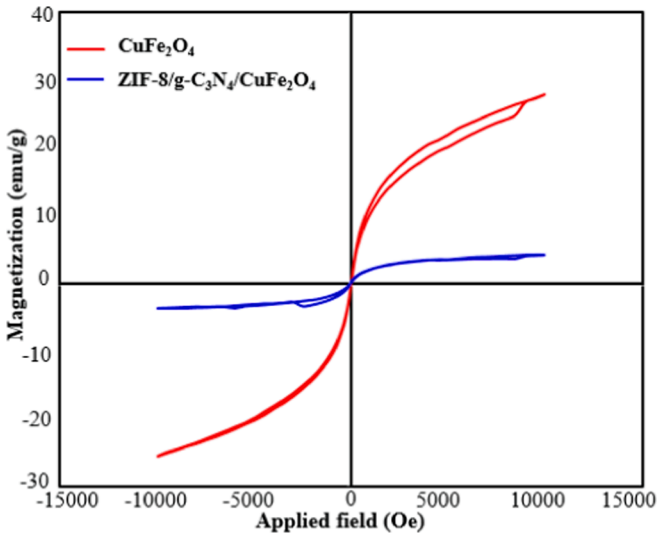

Fig. 4. Magnetic hysteresis loops of $CuFe_2O_4$, and ZIF-8/g-C_3N_4/$CuFe_2O_4$ nanocomposite (B).

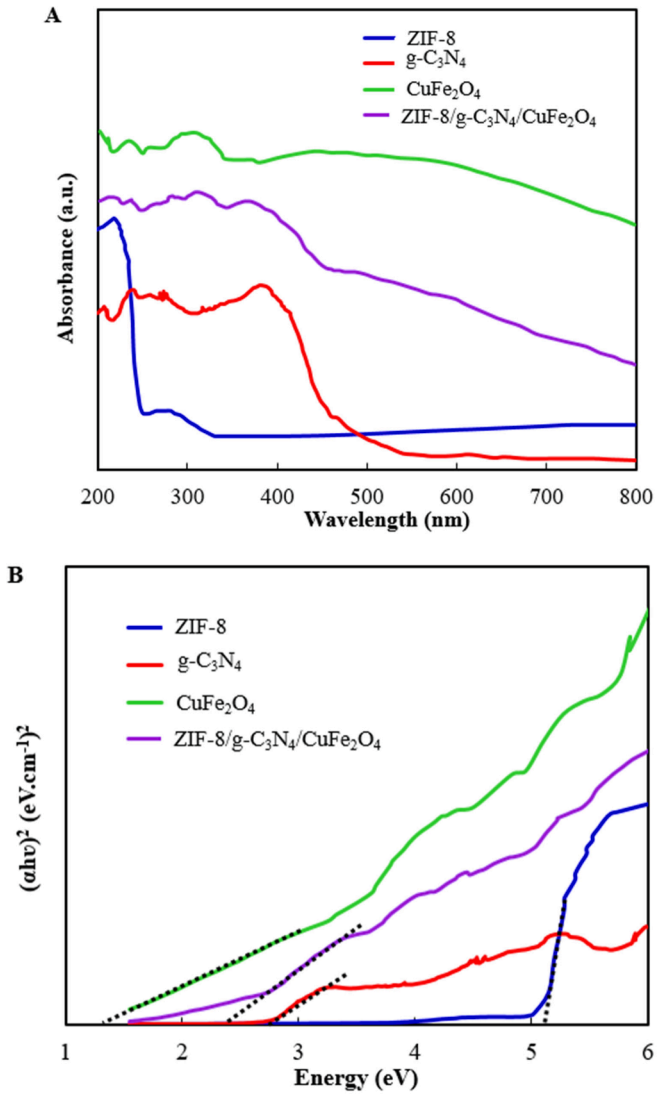

Fig. 5. Uv–Visible DRS spectra (A), and Tauc's plots (B), of ZIF-8, $CuFe_2O_4$, g-C_3N_4, and ZIF-8/g-C_3N_4/$CuFe_2O_4$ nanocomposite.

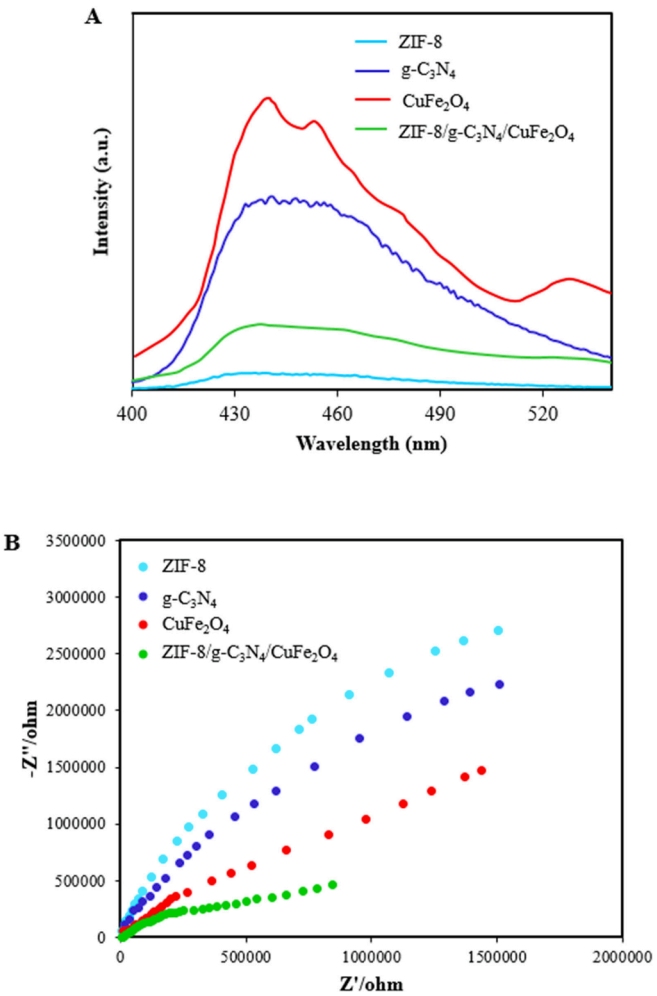

Fig. 6. PL spectra (A), and EIS Nyquist plots (B) of ZIF-8, g-C_3N_4, $CuFe_2O_4$, and ZIF-8/g-C_3N_4/$CuFe_2O_4$.

clear that ZIF-8/g-C_3N_4/$CuFe_2O_4$ has the smaller arc radius than ZIF-8, g-C_3N_4, and $CuFe_2O_4$, indicating the lower charge transfer resistance and as a result the photocatalytic activity is improved.

3.2. *Evaluations of photocatalytic activity*

The photocatalytic activity of the as-synthesized samples was examined by removal of TC under visible light. Fig. 7A shows the photodegradation of TC in the presence of ZIF-8, g-C_3N_4, $CuFe_2O_4$, ZIF-8/g-C_3N_4, ZIF-8/$CuFe_2O_4$, g-C_3N_4/$CuFe_2O_4$, and ZIF-8/g-C_3N_4/$CuFe_2O_4$ nanocomposite. As can be seen, for all samples the irradiation of visible light increases the TC degradation efficiency as compared to dark conditions. Therefore, visible light has an important role in the removal of TC from aqueous solution. On the other hand, after 65 min visible light irradiation, 25.09 %, 31.10 %, 21.23 %, 63.12 %, 49.03 %, 53.36 %, and, 94.71 % removal efficiencies were achieved for ZIF-8, g-C_3N_4, $CuFe_2O_4$, ZIF-8/g-C_3N_4, ZIF-8/$CuFe_2O_4$, g-C_3N_4/$CuFe_2O_4$, and ZIF-8/g-C_3N_4/$CuFe_2O_4$ nanocomposite, respectively. According to these results, the ZIF-8/g-C_3N_4/$CuFe_2O_4$ nanocomposite was shown excellent photocatalytic performance compared to other samples, which revealed a potent synergistic effect within the nanocomposite. In fact, the formed heterojunctions between ZIF-8, g-C_3N_4, and $CuFe_2O_4$ led to a decline in the rate of recombination of photo-induced electron-hole pairs and therefore, the photocatalytic activity improved.

In order to study the TC photodegradation rate by ZIF-8/g-C_3N_4/$CuFe_2O_4$ nanocomposite, a pseudo-first-order kinetic model was

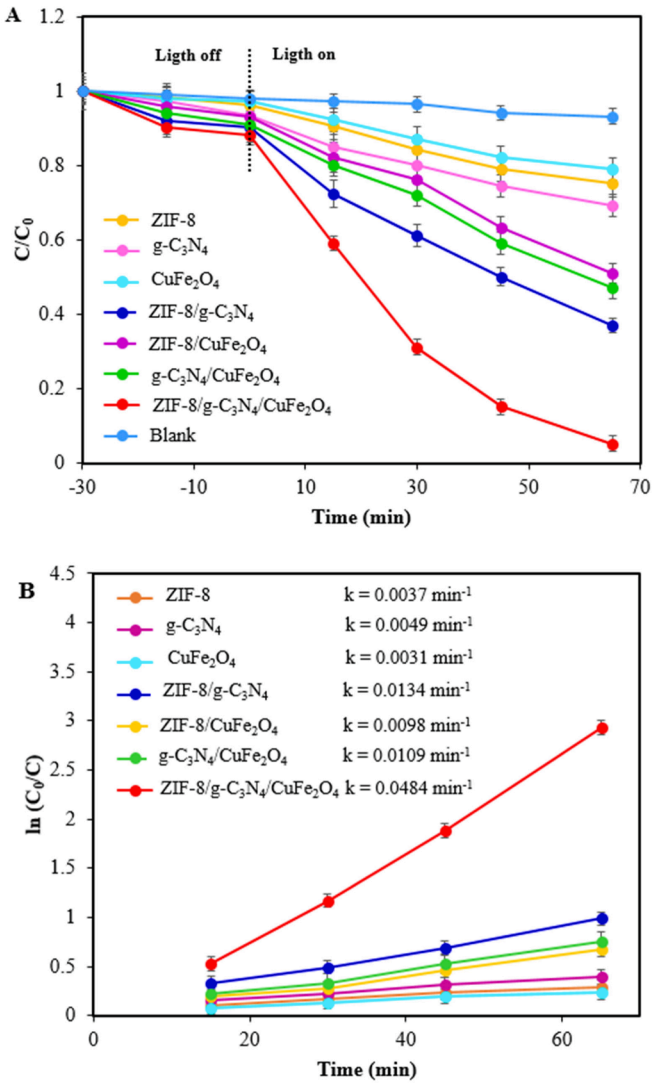

Fig. 7. Photocatalytic activities of ZIF-8, g-C_3N_4, $CuFe_2O_4$, ZIF-8/g-C_3N_4, ZIF-8/$CuFe_2O_4$, g-C_3N_4/$CuFe_2O_4$, and ZIF-8/g-C_3N_4/$CuFe_2O_4$ nanocomposite, under visible light irradiation (A), the corresponding kinetics of TC degradation (B) at constant amount of C_{TC}=15 ppm, $C_{Photocatalyst}$ = 0.75 g/L, and natural pH.

applied: ln (C_0/C_t) = kt, where C_0 refers to the initial concentration of TC, C_t is the TC concentration after t time of visible light irradiation, and k is the rate constant (Subash et al., 2023). Fig. 7B shows the kinetic fitting curves of TC photodegradation which were obtained using plotting ln (C_0/C_t) versus time. The results show a good linear relationship, therefore, the TC photodegradation follows from the pseudo-first-order kinetic model. The values of k for ZIF-8, g-C_3N_4, $CuFe_2O_4$, ZIF-8/g-C_3N_4, ZIF-8/$CuFe_2O_4$, g-C_3N_4/$CuFe_2O_4$ and ZIF-8/g-C_3N_4/$CuFe_2O_4$ nanocomposite were obtained 0.0037, 0.0049, 0.0031, 0.0134, 0.0098, 0.0109, and 0.0484 min^{-1}, respectively. Remarkably, ZIF-8/g-C_3N_4/$CuFe_2O_4$ nanocomposite has a maximum value of k, which is approximately 13.1, 9.9, 15.6, 3.6, 4.9, and 4.4 times higher than ZIF-8, g-C_3N_4, $CuFe_2O_4$, ZIF-8/g-C_3N_4, ZIF-8/$CuFe_2O_4$, and g-C_3N_4/$CuFe_2O_4$. The obtained results revealed that the photocatalytic activity of ZIF-8/g-C_3N_4/$CuFe_2O_4$ nanocomposite is remarkably increased.

3.3. Effect of operational parameters

The effect of three most important factors on the photodegradation efficiency including photocatalyst dosage, initial concentration of TC, and pH of solution were shown in Fig. 8A, B, and C. Various photocatalyst amounts of 0.45, 0.55, 0.67, and 0.75 g/L were applied to study the influence of photocatalyst dosage. As can be seen in Fig. 8A, by increasing the dosage of photocatalyst from 0.45 to 0.75 g/L, the photodegradation efficiency was enhanced due to an increase in the active site and amount of radical species. Therefore, the highest TC removal was achieved within 65 min reaction time using 0.75 g/L of ZIF-8/g-C_3N_4/$CuFe_2O_4$ nanocomposite. Fig. 8B reveals that if the initial concentration of TC increases from 15 to 45 ppm, the photocatalyst efficiency is decreased, because with increasing TC concentration, more active radicals are needed, while the amount of these radicals is constant due to the constant amount of photocatalyst. Also, by increasing initial TC concentration, the ratio between photocatalyst and TC molecules is decreased and as a result the ratio between the active sites on photocatalyst and TC molecules is decreased. On the other hand, in high concentrations of TC, the TC molecules cover the surface of nanocomposite and prevent the reaching of light to thephotocatalyst (Abinaya et al., 2023; Murugalakshmi et al., 2023; Govindan et al., 2019). Therefore, as a result, the photocatalytic performance was diminished. The effect of and solution pH were depicted in Fig. 8C. Based on zeta potential data (Fig. 8D), the pH_{zpc} of ZIF-8/g-C_3N_4/$CuFe_2O_4$ nanocomposite is 5.2, therefore the surface charge of nanocomposite is positive at pH values below 5.2 and negative at pH values above 5.2. On the other hand, TC has various chemical structures at different pHs. TC species are neutral in the pH range of 3.3 to 7.7, so there is no adsorption resistance between ZIF-8/g-C_3N_4/$CuFe_2O_4$ nanocomposite and TC, and the photocatalyst activity was improved. At the pH solution above 7.7, TC species were present as TCH^- and TC^{2-}, and due to electrostatic repulsion between TC and ZIF-8/g-C_3N_4/$CuFe_2O_4$ nanocomposite, the photocatalyst performance was decreased. Therefore, according to the results, pH 5 was selected as the optimum pH for TC removal.

3.4. Effect of interference

One of the important organic materials that found in municipal wastewater treatment plants is humic acid. During chlorine disinfection, humic acid can react with chlorine and form toxic byproducts. Fig. 9A was shown the effect of humic acid on the photocatalytic performance of ZIF-8/g-C_3N_4/$CuFe_2O_4$ for the degradation of TC. As can be seen in Figure, with the increase in the amount of humic acid the degradation efficiency of TC was decreased. In fact, by adding the humic acid the turbidity of the solution and affected the light transmittance was increased, and also humic acid competed with TC for surface sites of nanocomposite and active free radicals during the process. Therefore, as a result the degradation efficiency of TC was decreased. However, the photodegradation efficiencies for TC still reached 87.2 %, 83.01 %, and 75.5 % within 65 min, which reveal that the ZIF-8/g-C_3N_4/$CuFe_2O_4$ has great potential for the removal of TC in wastewater containing humic acid.

There are different ions occurring in wastewater, which can prevent the photocatalytic reaction because ions can quench the free radicals as well as occupy the active sites on the surface of the photocatalyst, and as a result affect the photodegradation efficiency. Therefore, different ions with concentrations of 10 mM were applied to investigate their influences on the photocatalytic process. As can be seen in Fig. 9B, various anions had a little effect on photocatalytic degradation efficiency, confirming that the photocatalyst has good tolerance for the ions in water.

3.5. Stability tests

The stability of the ZIF-8/g-C_3N_4/$CuFe_2O_4$ nanocomposite was evaluated, and the photodegradation efficiency for recycling was investigated under the same conditions. For this aim, after each run, ZIF-8/g-C_3N_4/$CuFe_2O_4$ photocatalyst was centrifuged, washed, and dried for the next runs. As exhibited in Fig. 10A, a small decrease in degradation efficiency was observed, which is probably due to the loss of trace

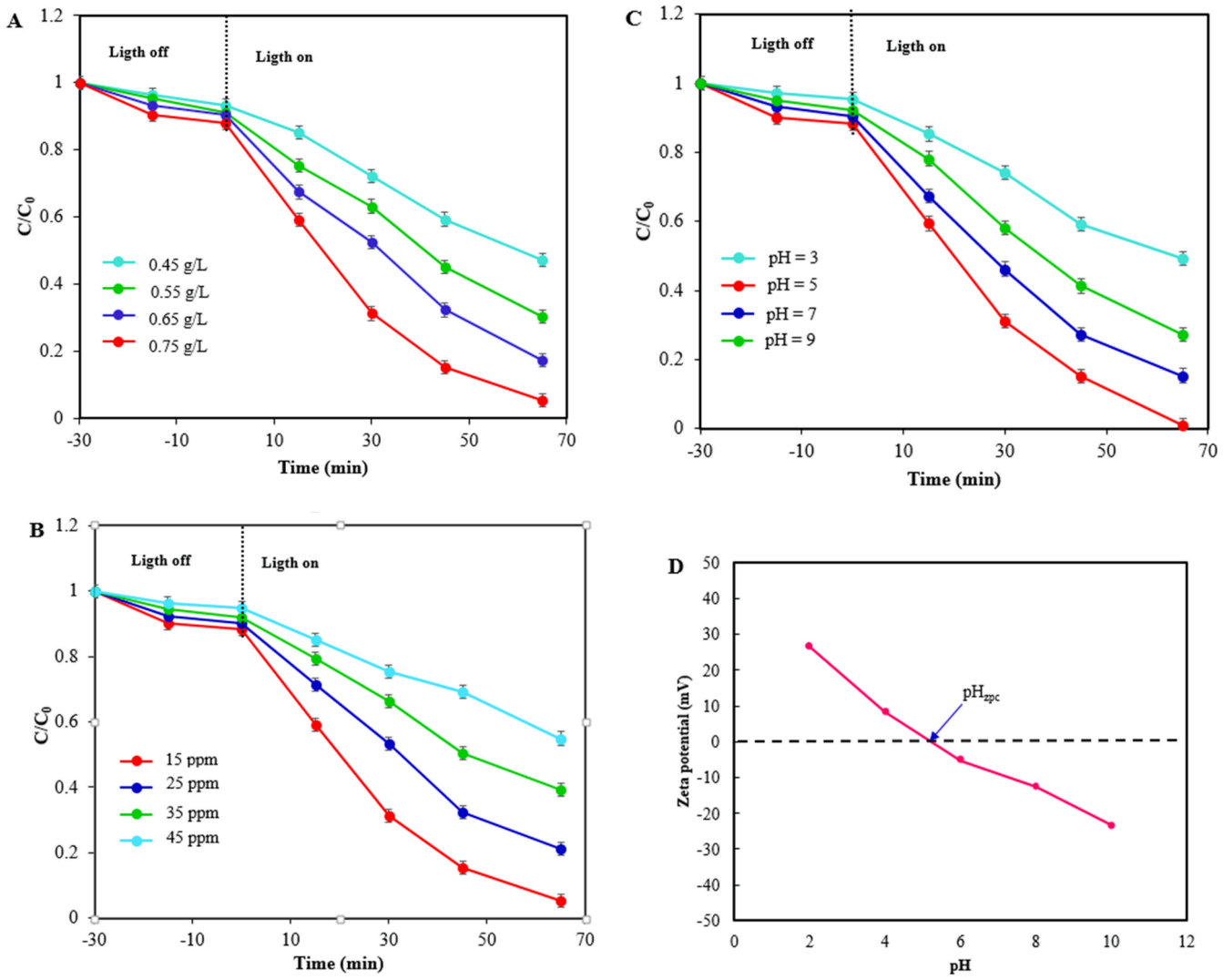

Fig. 8. Photodegradation of TC under visible light by ZIF-8/g-C_3N_4/$CuFe_2O_4$ at various photocatalyst dosages with constant amount of C_{TC}=15 ppm, and natural pH (A), various initial TC concentration with constant amount of $C_{Photocatalyst}$ = 0.75 g/L, and natural pH (B), at various pH with constant amount of $C_{Photocatalyst}$ = 0.75 g/L, and C_{TC}=15 ppm (C),and zeta potential of ZIF-8/g-C_3N_4/$CuFe_2O_4$ (D) at different solution pHs.

amount of nanocomposite during its separation and also deposition of by-products or intermediates on the surface of photocatalyst (Kumar et al., 2021). Therefore, the proposed photocatalyst shows excellent recyclability for degradation of TC and seems to be an economical photocatalyst for TC removal from wastewater.

The amount of leached Fe and Cu elements from ZIF-8/g-C_3N_4/$CuFe_2O_4$ was studied for 4 cycles. The results (Table 1) exhibited that the leached Fe and Cu elements was insignificant, indicating a high physicochemical stability for ZIF-8/g-C_3N_4/$CuFe_2O_4$ in photocatalyst process.

To further confirm the stability of ZIF-8/g-C_3N_4/$CuFe_2O_4$ during the photocatalyst process, the XRD pattern of ZIF-8/g-C_3N_4/$CuFe_2O_4$ nanocomposite was recorded after four cycles. As exhibited in Fig. 10B, crystal structure of ZIF-8/g-C_3N_4/$CuFe_2O_4$ nanocomposite has no significant changes, which indicate its excellent stability.

3.6. TOC analysis

In order to confirm the mineralization of TC on ZIF-8/g-C_3N_4/$CuFe_2O_4$ nanocomposite under visible light irradiation, the change of total organic carbon content (TOC) was monitored. As illustrated in Fig. 11A, with the progress of the photodegradation process, the TOC value of the reaction solution declines gradually. The measured initial TOC (TOC_0) was obtained 39.82 mg/L, and after 65 min of photodegradation reaction TOC was measured 17.12 mg/L with a mineralization degree of 55.75 %, revealing that ZIF-8/g-C_3N_4/$CuFe_2O_4$ nanocomposite can efficiently mineralize TC.

3.7. Photocatalytic mechanism

To detect the active species in the process of TC photodegradation, trapping experiments were performed using benzoquinone (BQ), isopropanol (IPA), and disodium ethylenediaminetetraacetic acid (EDTA-2Na), as scavengers for superoxide ions ($\cdot O_2^-$), hydroxyl radicals ($\cdot OH$), and holes (h^+). BQ is a good scavenger for $\cdot O_2^-$, and it can react with $\cdot O_2^-$ at a constant rate of $9 \times 10^8\ M^{-1}\ S^{-1}$ (Sargazi et al., 2019). After addition of BQ the constant rate of photocatalytic degradation was decreased from 0.0484 min^{-1} to 0.0245 min^{-1}. Also, as a scavenger, IPA can react with $\cdot OH$ at a constant rate of $1.9 \times 10^9\ M^{-1}\ S^{-1}$ (Makama et al., 2020). In the presence of IPA, the reaction rate decreased to 0.0102 min^{-1}. EDTA-2Na usually assumed as an effective quencher holes and it can be decreas the reaction rate to 0.006 min^{-1} from a high constant rate of 0.0484 min^{-1}. As illustrated in Fig. 11B, the photocatalytic activity of ZIF-8/g-C_3N_4/$CuFe_2O_4$ nanocomposite was inhibited greatly by the addition of EDTA-2Na and IPA, while the addition of the BQ had less impact on the

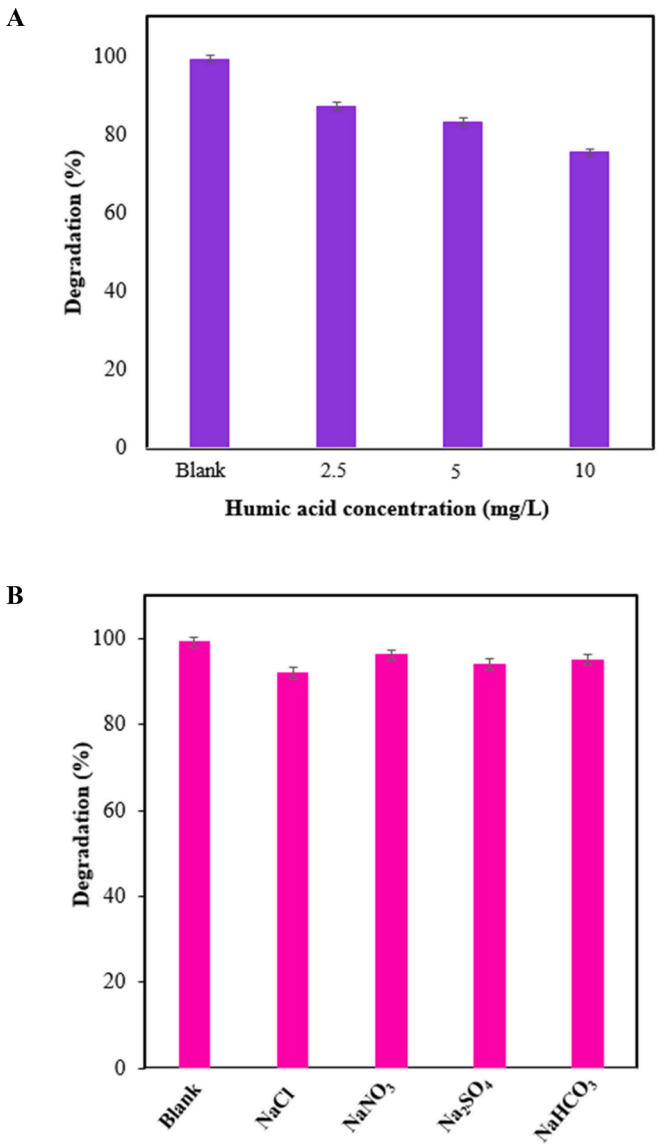

Fig. 9. Effect of humic acid (A), and ions (B) on the photodegradation efficiency of TC by ZIF-8/g-C_3N_4/$CuFe_2O_4$ ($C_{Photocatalyst}$ = 0.75 g/L, C_{TC}=15 ppm, and pH=5).

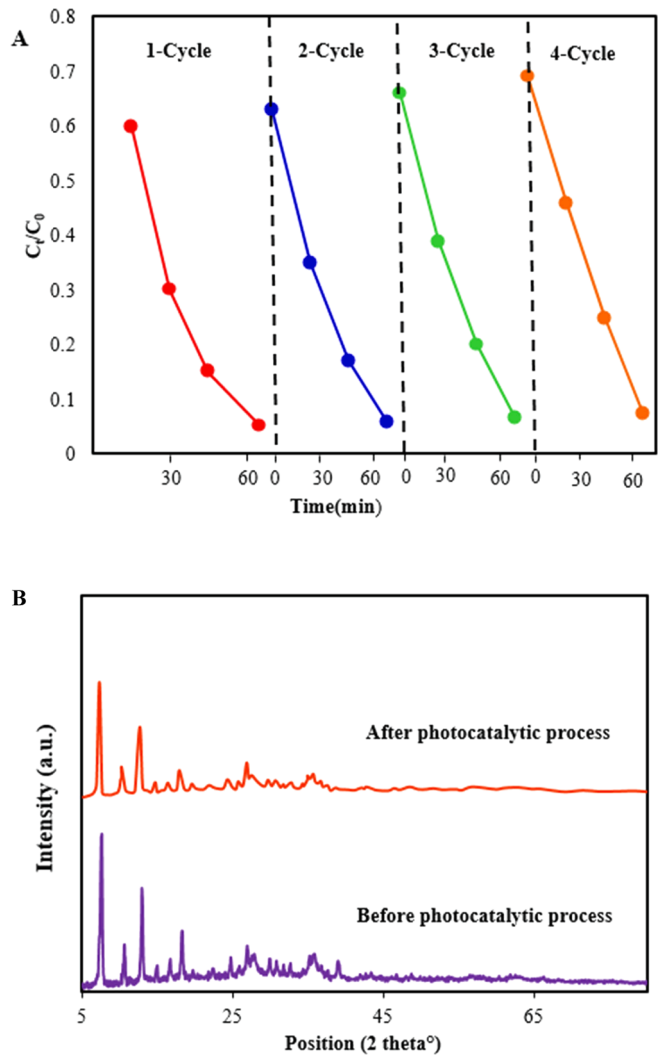

Fig. 10. Recycling tests for photodegradation of TC over ZIF-8/g-C_3N_4/$CuFe_2O_4$ at constant amount of C_{TC}=15 ppm, $C_{Photocatalyst}$ = 0.75 g/L, and pH=5 (A), and comparison XRD pattern of ZIF-8/g-C_3N_4/$CuFe_2O_4$ before and after photocatalyst process.

Table 1
Cu and Fe leaching from the first use to fourth run.

Element	Number of cycles/Cu or Fe leaching (mg/L)			
	1	2	3	4
Cu	0.20	0.09	0.05	0.001
Fe	0.28	0.12	0.08	0.03

photocatalytic performance. Therefore, h^+ and·OH are the primary active species, and·O_2^- plays a smaller role in the TC photodegradation process.

ESR was used to further confirm the effect of active species. To quenching h^+, TEMPO was applied as well as to quenching·O_2^- and ·OH, DMPO was used. As shown in Fig. 12A, after turn on the light, the signal peak of h^+ weakened because h^+ reacted with TEMPO and produce a spin adduct (TEMPO- h^+); this result reveals that h^+ was involved in the photodegradation reaction as an active free radical. Also, as can be seen in Fig. 12B, the ESR spectrum of ZIF-8/g-C_3N_4/$CuFe_2O_4$ nanocomposite in DMPO solution under visible light irradiation displays four characteristic peaks with an intensity ratio of 1:2:2:1, which is a typical peak of DMPO-·OH. In addition, Fig. 12C displays a quartet-line ESR signal related to·O_2^- for ZIF-8/g-C_3N_4/$CuFe_2O_4$ nanocomposite, where the intensity ratio was 1:1:1:1. Moreover, as can be seen in Fig. 12B and C, in the absence of light, no characteristic DMPO-·O_2^- and DMPO-·OH signals was detected, revealing that the·O_2^- radicals and ·OH radicals can only be produced under visible-light irradiation. Also, we note that the signal intensity of the characteristic peak •OH was more notable, indicating that more •OH generated and played a more significant role in the photocatalytic degradation of TC. This result was consistent with the results of the free radical trapping experiments.

The potentials of the conduction band (E_{CB}), and valence band (E_{VB}) of semiconductors were calculated according to the empirical formula as follows (Long et al., 2006):

$$E_{VB} = \chi - E_e + 0.5E_g$$

$$E_{CB} = E_{VB} - E_g$$

Where, E_e and χ denote the potential of standard hydrogen electrode (~4.5 eV), and the absolute electronegativity of the semiconductor. E_g is the energy of the band gap of each semiconductor. The calculated values E_{VB} for ZIF-8, g-C_3N_4, $CuFe_2O_4$ are 4.22 eV, 1.57 and 1.96 eV,

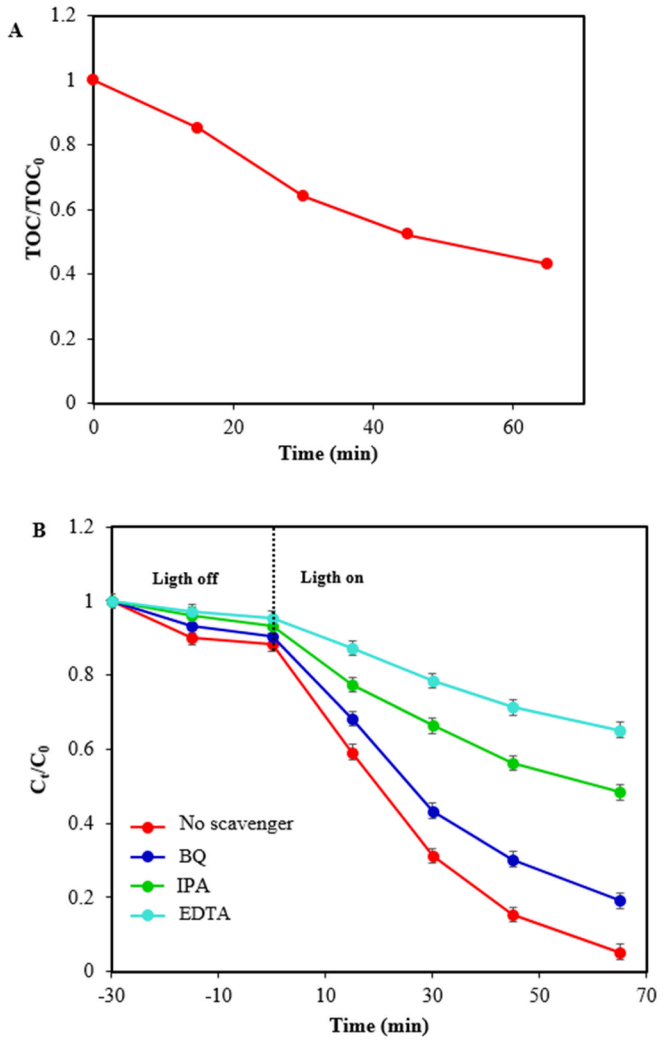

Fig. 11. Change of TOC during TC photodegradation (A), and effect of various scavengers on TC photodegradation over ZIF-8/g-C_3N_4/$CuFe_2O_4$ with constant amount of $C_{Photocatalyst}$ = 0.75 g/L, C_{TC}=15 ppm, and pH=5 (B).

respectively. Also, the E_{CB} for ZIF-8, g-C_3N_4, and $CuFe_2O_4$ were estimated to be −0.88 eV, −1.11 eV, and 0.66 eV, respectively. Fig. 13 exhibited the band distribution of the ZIF-8, g-C_3N_4, and $CuFe_2O_4$. Under visible light irradiation, the electrons were excited in g-C_3N_4, and $CuFe_2O_4$. Therefore, the CBs and VBs of g-C_3N_4, and $CuFe_2O_4$ were repositioned the electron-rich and hole-rich, respectively. However, ZIF-8 cannot excited by visible light irradiation due to the wide band gap energy therefore, the electron-hole pairs are impossible to form. The CB of ZIF-8, g-C_3N_4, and $CuFe_2O_4$ are more negative than the standard redox potential of O_2/H_2O_2 which is 0.685 eV vs. NHE. Therefore, the electrons in the CB of the semiconductors react with the O_2 and generate H_2O_2 and then electrons combine with H_2O_2 to form·OH with strong oxidation ability. The CB of ZIF-8 and g-C_3N_4 are more negative than the standard redox potential of $O_2/{}^{\cdot}O_2^-$ which is − 0.33 eV vs. NHE. Therefore, O_2 can reduced to·O_2^-, which is in agreement with the scavengers experiment results. Furthermore, the holes in the VB of ZIF-8 can participate directly in the photodegradation process due to their strong oxidizing power.

According to the above results, the progress of tTC degradation under visible light is as follows (Yue et al., 2024; Subash et al., 2023):

ZIF-8/g-C_3N_4/$CuFe_2O_4$ + $h\nu$ (visible light) → ZIF-8/g-C_3N_4/$CuFe_2O_4$ (e^-_{CB}, h^+_{VB})

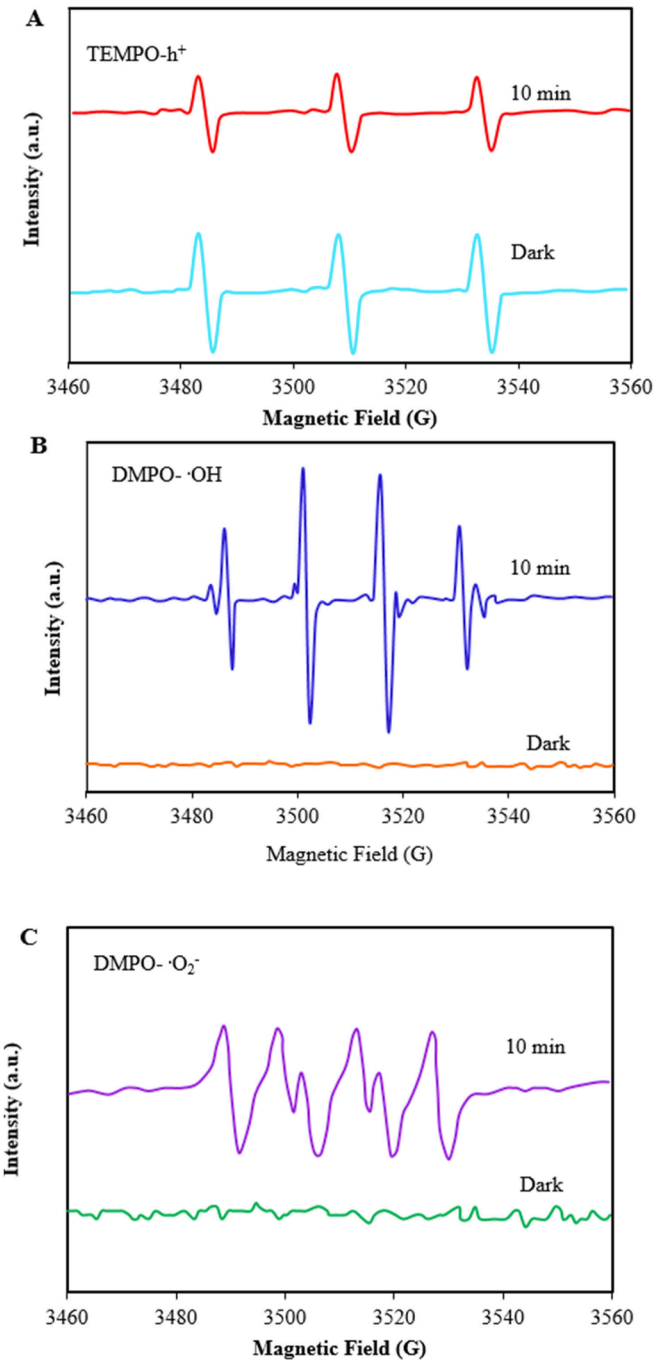

Fig. 12. ESR spectra of TEMPO-h^+ (A), DMPO-·OH (B), and DMPO-·O_2^-(C).

ZIF-8/g-C_3N_4/$CuFe_2O_4$ (h^+_{VB}) + H_2O→OH^- +·OH

ZIF-8/g-C_3N_4/$CuFe_2O_4$ (h^+_{VB}) + OH^- →·OH

ZIF-8/g-C_3N_4/$CuFe_2O_4$ (e^-_{CB})+ ½ O_2 + H^+ → H_2O_2

ZIF-8/g-C_3N_4/$CuFe_2O_4$ (e^-_{CB}) + H_2O_2 → OH^- +·OH

ZIF-8/g-C_3N_4/$CuFe_2O_4$ (e^-_{CB}) + O_2 →·O_2^-

·OH, ZIF-8/g-C_3N_4/$CuFe_2O_4$ (h^+_{VB}) + TC→Degradation products

3.8. Comparison with other photocatalyst

The efficiency of the as-synthesized ZIF-8/g-C_3N_4/$CuFe_2O_4$ as a

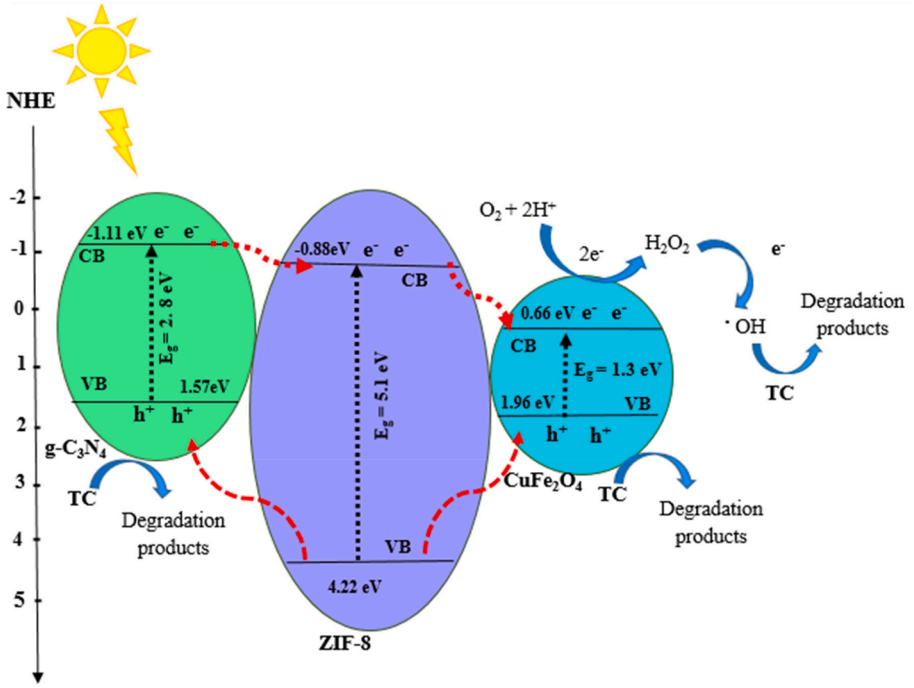

Fig. 13. Proposed photocatalytic mechanism of TC over the ZIF-8/g-C_3N_4/$CuFe_2O_4$.

photocatalyst was compared with other reported photocatalysts listed in Table 2. The comparison show that, ZIF-8/g-C_3N_4/$CuFe_2O_4$ has higher photocatalytic activity, and k value other reported photocatalysts. These results reveal the great potential of new ZIF-8/g-C_3N_4/$CuFe_2O_4$ photocatalyst for removal of TC from aqueous solution.

4. Conclusion

The novel ZIF-8/g-C_3N_4/$CuFe_2O_4$ nanocomposite was prepared by a facile and low-cost impregnation method. The photocatalytic activities of the as-synthesized samples were examined by photodegradation of TC under visible light irradiation. Results exhibit that the ZIF-8/g-C_3N_4/$CuFe_2O_4$ heterostructures showed higher photocatalytic activity than pristine ZIF-8, g-C_3N_4, and $CuFe_2O_4$. The removal efficiency of ZIF-8/g-C_3N_4/$CuFe_2O_4$ nanocomposite increased by up to 99.15 %, after 65 min visible light irradiation. The results of the recycling test show that the used photocatalyst could be magnetically separated from solutions for the next run. The used nanocomposite still has reasonable photocatalytic activity. The results of recycling tests exhibit that magnetically separable ZIF-8/g-C_3N_4/$CuFe_2O_4$ photocatalysts have good reusability and stability. The formation of the ZIF-8/g-C_3N_4/$CuFe_2O_4$ in the nanocomposite can improve the absorption of solar light and promote the separation of charge carriers, which remarkably increases its photocatalytic performances under solar irradiation.

Table 2
Comparison between ZIF-8/g-C_3N_4/$CuFe_2O_4$ photocatalyst and other materials for the degradation of TC.

Potocatalyst	Dosage (g/L)	TC conc. (ppm)	Time (min)	%D	Rate constant (min^{-1})	References
WO_3/g-C_3N_4/Bi_2O_3	1	10	60	80.2	0.0236	(Jiang et al., 2018)
B-TiO_2/$BiVO_4$	0.5	20	120	89.30	0.0484	(Wu et al., 2023)
MgAl-LDH/$(BiO)_2CO_3$	1	15	105	97.2	0.02059	(Sun et al., 2022)
TiO_2/$Ti_3C_2T_x$/AgI	1	20	180	97	0.017	(Wu et al., 2022)
CFs/g-C_3N_4/BiOBr	3	20	120	86.1	0.015	(Shi et al., 2020)
Ag/Ag_2CO_3/$BiVO_4$	1	20	150	94.9	0.0186	(Liu et al., 2018)
h-BN/g-C_3N_4	1	10	60	79.7	0.0277	(Xia et al., 2019)
ZIF-8/g-C3N4/CuFe2O4	0.75	15	65	99.15	0.0484	This work

CRediT authorship contribution statement

Anjan Kumar: Writing – original draft, Software, Investigation, Formal analysis, Data curation. **Ali M. Hussein:** Writing – original draft, Validation, Software, Resources, Methodology, Investigation, Formal analysis, Conceptualization. **Farag M.A. Altalbawy:** Writing – review & editing, Visualization, Validation, Supervision, Software, Resources, Data curation. **Mandeep Kaur:** Writing – review & editing, Supervision, Software, Resources, Project administration. **Harpreet Kaur:** Software, Methodology, Investigation, Formal analysis, Data curation. **Sarah Salah Jalal:** Writing – original draft, Software, Resources, Methodology, Investigation, Formal analysis. **Salah Hassan Zain Al-Abdeen:** Writing – review & editing, Visualization, Supervision, Resources, Funding acquisition, Conceptualization. **Khursheed Muzammil:** Writing – review & editing, Visualization, Validation, Supervision, Project administration, Funding acquisition. **Merwa Alhadrawi:** Writing – review & editing, Visualization, Validation, Supervision, Resources, Project administration, Funding acquisition.

Declaration of competing interest

The authors declare that they have no known competing financial interests or personal relationships that could have appeared to influence the work reported in this paper.

Acknowledgment

The authors extend their appreciation to the Deanship of Research and Graduate Studies at King Khalid University, KSA, for funding this work through a large research group program under grant number RGP. 2/220/45.

References

Abdi, J., 2020. Synthesis of Ag-doped ZIF-8 photocatalyst with excellent performance for dye degradation and antibacterial activity. Colloids Surf. a: Physicochem. Eng. Asp. 604, 125330.

Abinaya, M., Govindan, K., Kalpana, M., Saravanakumar, K., Prabavathi, S.L., Muthuraj, V., Jang, A., 2023. Reduction of hexavalent chromium and degradation of tetracycline using a novel indium-doped Mn_2O_3 nanorod photocatalyst. J. Hazard. Mater. 397, 122885.

Ammar, S.H., Hadi, H.J., Abdul-wahid, I.K., Jabbar, Z.H., 2023. Visible-light boosted photocatalytic performance of sulfonated polypyrrole-coated ZIF-8 hybrids for pollutants degradation. J. Mol. Struct. 1288, 135752.

Baaloudj, O., Assadi, I., Nasrallah, N., El Jery, A., Khezami, L., Assadi, A.A., 2021. Simultaneous removal of antibiotics and inactivation of antibiotic-resistant bacteria by photocatalysis: A review. J. Water Proc.engineering 42, 102089.

Cai, H., Ma, Z., Zhao, T., 2021. Fabrication of magnetic $CuFe_2O_4$@ PBC composite and efficient removal of metronidazole by the photo-Fenton process in a wide pH range. J. Environ. Manag. 300, 113677.

Chen, Y., Pu, S., Wang, D., Zhang, Y., Wan, G., Zhao, Q., Sun, Y., 2023. Facile synthesis of AgBr@ZIF-8 hybrid photocatalysts for degradation of Rhodamine B. J. Solid State Chem. 321, 123857.

Chen, G., Yu, Y., Liang, L., Duan, X., Li, R., Lu, X., Yan, B., Li, N., Wang, S., 2021. Remediation of antibiotic wastewater by coupled photocatalytic and persulfate oxidation system: A critical review. J. Hazard. Mater. 408, 124461.

Chin, J.Y., Ahmad, A.L., Low, S.C., 2023. Evolution of photocatalytic membrane for antibiotics degradation: Perspectives and insights for sustainable environmental remediation. J. Water Proc.engineering. 51, 103342.

da Silva, F.F., da Silva, R.B., Silva, T.R., de Macedo, D.A., Su, B., 2023. Boosting the photocatalytic activity of g-C_3N_4/ZnO heterojunctions through optimal control of mass ratio. Solid State Sci. 138, 107128.

Davies, K.R., Cherif, Y., Pazhani, G.P., Anantharaj, S., Azzi, H., Terashima, C., Fujishima, A., Pitchaimuthu, S., 2021. The upsurge of photocatalysts in antibiotic micropollutants treatment: Materials design, recovery, toxicity and bioanalysis. J. Photochem. Photobiol. c: Photochem. Rev. 48, 100437.

Ding, C., Zhu, Q., Yang, B., Petropoulos, E., Xue, L., Feng, Y., He, S., Yang, L., 2023. Efficient photocatalysis of tetracycline hydrochloride (TC-HCl) from pharmaceutical wastewater using AgCl/ZnO/g-C_3N_4 composite under visible light: Process and mechanisms. J. Environ. Sci. 126, 249–262.

El Messaoudi, N., Ciğeroğlu, Z., Mine Şenol, Z., Elhajam, M., Noureen, L., 2023. A comparative review of the adsorption and photocatalytic degradation of tetracycline in aquatic environment by g-C_3N_4-based materials. J. Water Proc. engineering 55, 104150.

Govindan, K., Murugesan, S., Maruthamuthu, P., 2013. Photocatalytic degradation of pentachlorophenol in aqueous solution by visible light sensitive NF-codoped TiO_2 photocatalyst. Mater. Res. Bull. 48, 1913–1919.

Govindan, K., Chandran, H.T., Raja, M., Maheswari, S.U., Rangarajan, M., 2017. Electron scavenger-assisted photocatalytic degradation of amido black 10B dye with Mn_3O_4 nanotubes: a response surface methodology study with central composite design. J. Photochem. Photobio a: Chem. 341, 146–156.

Govindan, K., Suresh, A.K., Sakthivel, T., Murugesan, K., Mohan, R., Gunasekaran, V., Jang, A., 2019. Effect of peroxomonosulfate, peroxodisulfate and hydrogen peroxide on graphene oxide photocatalytic performances in methyl orange dye degradation. Chemosphere 237, 124479.

Gowriboy, N., Kalaivizhi, R., Ganesh, M.R., K.a., 2022. AswathyDevelopment of thin film polymer nanocomposite membrane (ZIF-8@ PSf/CS) for removal of textile pollutant and evaluating the effect of water samples on human monocytic cell lines (THP-1) using flow cytometer. J. Clean. Prod. 377, 134399.

Hayat, A., Sohail, M., Anwar, U., Taha, T.A., Qazi, H.I.A., Amina, Z., Ajmal, A.G., Al-Sehemi, H., Algarni, A.A., Al-Ghamdi, M.A., Amin, A., Palamanit, W.I., Nawawi, E.F., Newair, Y.O., 2023. A Targeted Review of Current Progress, Challenges and Future Perspective of g-C_3N_4 based Hybrid Photocatalyst Toward Multidimensional Applications. Chem. Rec. 23, 202200143.

Heris, S.Z., Etemadi, M., Mousavi, S.B., Mohammadpourfard, M., Ramavandi, B., 2023. Preparation and characterizations of TiO_2/ZnO nanohybrid and its application in photocatalytic degradation of tetracycline in wastewater. J. Photochem. Photobiol. a: Chem. 443, 114893.

Hong, Y., Wang, B., Hu, S., Lu, S., Wu, Q., Fu, M., 2023. Chenzhang Gu, and Yinzhen Wang, Preparation and photocatalytic performance of Zn_2SnO_4/ZIF-8 nanocomposite. Ceram. Int. 49, 11027–11037.

Hu, C., Chu, Y.C., Wang, M.S., Wu, X.H., 2017. Rapid synthesis of g-C_3N_4 spheres using microwave-assisted solvothermal method for enhanced photocatalytic activity. J. Photochem. Photobiol. a: Chem. 348, 8–17.

Hu, M., Zhao, D., Yan, X., Hu, X., Zhou, M., Shu, Y., Liu, P., 2024. Construction of Z-scheme heterojunction ZIF-8-decorated ZnO/SiO_2 for enhanced visible-light photocatalytic removal of organic pollutants and reduction of Cr (VI). Appl. Surf. Sci. 160321.

Jiang, L., Yuan, X., Zeng, G., Liang, J., Chen, X., Yu, H., Wang, H., Wu, Z., Zhang, J., Xiong, T., 2018. T, In-situ synthesis of direct solid-state dual Z-scheme WO_3/g-C_3N_4/Bi_2O_3 photocatalyst for the degradation of refractory pollutant. Appl. Catal. b. 227, 376–385.

Khan, I., Wang, C., Khan, S., Chen, J., Khan, A., Shah, S.A., Yuan, A., Khan, S., Butt, M.K., Asghar, H., 2023. Bio-capped and green synthesis of ZnO/g-C_3N_4 nanocomposites and its improved antibiotic and photocatalytic activities: An exceptional approach towards environmental remediation. Chin. J. Chem. Eng. 56, 215–224.

Kumar, R.S., Govindan, K., Ramakrishnan, S., Kim, A.R., Kim, J.S., Yoo, D.J., 2021. Fe_3O_4 nanorods decorated on polypyrrole/reduced graphene oxide for electrochemical detection of dopamine and photocatalytic degradation of acetaminophen. Appl. Surf. Sci. 556, 149765.

Li, R., Li, W., Jin, C., He, Q., Wang, Y., 2020. Fabrication of ZIF-8@ TiO_2 micron composite via hydrothermal method with enhanced absorption and photocatalytic activities in tetracycline degradation. J. Alloys Comp. 825, 154008.

Li, W., Ma, X., Huang, G., Lian, R., Huang, J., She, H., Wang, Q., 2022. Construction of ternary CuO/$CuFe_2O_4$/g-C_3N_4 composite and its enhanced photocatalytic degradation of tetracycline hydrochloride with persulfate under simulated sunlight. J. Environ. Sci. 112, 59–70.

Li, J., Tian, T., Jia, Y., Xu, N., Yang, S., Zhang, C., Gao, S., Shen, W., Wang, Z., 2023. Adsorption performance and optimization by response surface methodology on tetracycline using Fe-doped ZIF-8-loaded multi-walled carbon nanotubes. Environ. Sci. Pollut. Res. Int. 30, 4123–4136.

Li, S., Wang, C., Liu, Y., Xue, B., Jiang, W., Liu, Y., Mo, L., Chen, X., 2021. Photocatalytic degradation of antibiotics using a novel $Ag/Ag_2S/Bi_2MoO_6$ plasmonic pn heterojunction photocatalyst: Mineralization activity, degradation pathways and boosted charge separation mechanism Chem. Eng. J. 415, 128991.

Li, D., Yang, J., Lv, S., Li, X., Shao, L., Zhou, C., Xu, F., 2023. Insights into the degradation mechanisms of TCH by magnetic Fe_3S_4/Cu_2O composite. Inorg. Chem. 62, 10713–10726.

Liu, J., Meng, C., Zhang, X., Wang, S., Duan, K., Li, X., Hu, Y., Cheng, H., 2023. Direct Z-scheme In_2O_3/AgI heterojunction with oxygen vacancies for efficient molecular oxygen activation and enhanced photocatalytic degradation of tetracycline. Chem. Eng. J. 466, 143319.

Liu, J., Dong, Y., Liu, Q., Liu, W., Lin, H., 2024. MoS_2-based nanocomposites and aerogels for antibiotic pollutants removal from wastewater by photocatalytic degradation process: A review. Chemosphere 141582.

Liu, Y., Kong, J., Yuan, J., Zhao, W., Zhu, X., Sun, C., Xie, J., 2018. Enhanced photocatalytic activity over flower-like sphere $Ag/Ag_2CO_3/BiVO_4$ plasmonic heterojunction photocatalyst for tetracycline degradation. J. Chem. Eng. 331, 242–254.

M. Long, W. Cai, J. Cai, B. Zhou, X. Chai, Y. Wu, Efficient photocatalytic degradation of phenol over $Co_3O_4/BiVO_4$ composite under visible light irradiation. J. Phys. Chem. B 110 (2006) 20211-20216.\.

Luo, J., Wu, Y., Jiang, M., Zhang, A., Chen, X., Zeng, Y., Wang, Y., Zhao, Y., Wang, G., 2023. Novel $ZnFe_2O_4$/BC/ZnO photocatalyst for high-efficiency degradation of tetracycline under visible light irradiation. Chemosphere 311, 137041.

Makama, A.B., Salmiaton, A., Choong, T.S.Y., Hamid, M.R.A., Abdullah, N., Saion, E., 2020. Influence of parameters and radical scavengers on the visible-light-induced degradation of ciprofloxacin in ZnO/SnS_2 nanocomposite suspension: Identification of transformation products. Chemosphere 253, 126689.

Mittal, H., Ivaturi, A., Khanuja, M., 2023. $MoSe_2$-modified ZIF-8 novel nanocomposite for photocatalytic remediation of textile dye and antibiotic-contaminated wastewater. Environ. Sci. Pollut. Res. 30, 4151–4165.

Motora, K.G., Wu, C.M., Lin, S.T., 2023. Novel Ag_3PO_4@ZIF-8 pn heterojunction for effective photodegradation of organic pollutants. J. Water Proc. Engineering 52, 103586.

Murugalakshmi, M., Govindan, K., Umadevi, M., Breslin, C.B., Muthuraj, V., 2023. Fabrication of a Sm_2O_3/In_2S_3 photocatalyst for boosting ciprofloxacin oxidation and the Cr (vi) reduction: process parameters and degradation mechanism. Environ. Sci.: Water Res. Technol. 9, 1385–1402.

Palanivel, B., Ayappan, C., Jayaraman, V., Chidambaram, S., Maheswaran, R., Mani, A., 2019. Inverse spinel $NiFe_2O_4$ deposited g-C_3N_4 nanosheet for enhanced visible light photocatalytic activity. Mater. Sci. Semicond. Process. 100, 87–97.

Pattanayak, D.S., Pal, D., Mishra, J., Thakur, C., 2023. Noble metal–free doped graphitic carbon nitride (g-C_3N_4) for efficient photodegradation of antibiotics: progress, limitations, and future directions. Environ. Sci. Pollut. Res. 30, 25546–25558.

Qiu, M., Xu, W., Chen, S., Jia, Z., Li, Y., He, J., Wang, L., Lei, J., Liu, C., Liu, J., 2023. A novel adsorptive and photocatalytic system for dye degradation using ZIF-8 derived carbon (ZIF-C)-modified graphene oxide nanosheets. J. Taiwan Inst. Chem. Eng. 143, 104674.

Rabeie, B., Mahmoodi, N.M., 2023. Hierarchical ternary titanium dioxide decorated with graphene quantum dot/ZIF-8 nanocomposite for the photocatalytic degradation of doxycycline and dye using visible light. J. Water Proc. Engineering 54, 103976.

Ramadevi, P., Vinodhkumar, G., Shanmugavadivu, R., 2023. An efficient visible light driven photocatalyst based on $CuFe_2O_4$/rGO nanocomposites for effective degradation of methylene blue dye. Optik 277, 170713.

Ranjithkumar, R., Lakshmanan, P., Devendran, P., Nallamuthu, N., Sudhahar, S., Krishna Kumar, M., 2021. Investigations on effect of graphitic carbon nitride loading on the properties and electrochemical performance of g-C_3N_4/TiO_2 nanocomposites for energy storage device applications. Mater. Sci. Semicond. Process. 121, 105328.

Rouibah, K., Akika, F.Z., Rouibah, C., Boudermine, H.R., Douafer, S., Boukerche, S., Boukerche, G., Benamira, M., 2023. Solar photocatalytic degradation of Methyl green on $CuFe_2O_4$/αFe_2O_3 heterojunction. Inorg. Chem. Commun. 148, 110361.

Sargazi, G., Afzali, D., Mostafavi, A., 2019. A novel microwave assisted reverse micelle fabrication route for Th (IV)-MOFs as highly efficient adsorbent nanostructures with

controllable structural properties to CO and CH4 adsorption: Design, and a systematic study. Appl. Organomet. Chem. 33 (4), e4816.
Shi, Z., Zhang, Y., Shen, X., Duoerkun, G., Zhu, B., Zhang, L., Li, M., Chen, Z., 2020. Fabrication of g-C_3N_4/BiOBr heterojunctions on carbon fibers as weaveable photocatalyst for degrading tetracycline hydrochloride under visible light. Chem. Eng. J. 386, 124010.
Song, P., Xu, B., Yang, Q., Wang, D., Yang, P., 2024. Alkaline metal derived secondary thermal polymerization for superior thin g-C_3N_4 nanosheets with efficient photocatalytic performance. Int. J. Hydrogen Energy 51, 425–435.
Subash, M., Chandrasekar, M., Panimalar, S., Inmozhi, C., Parasuraman, K., Uthrakumar, R., Kaviyarasu, K., 2023. Pseudo-first kinetics model of copper doping on the structural, magnetic, and photocatalytic activity of magnesium oxide nanoparticles for energy application. Biomass Convers. Biorefin. 13, 3427–3437.
Sun, C., Wang, Y., Wu, L., Hu, J., Long, X., Wu, H., Jiao, F., 2022. In situ preparation of novel p–n junction photocatalyst MgAl-LDH/$(BiO)_2CO_3$ for enhanced photocatalytic degradation of tetracycline. Mater. Sci. Semicond. Process. 150, 106939.
Sun, S., Yang, Z., Cao, J., Wang, Y., Xiong, W., 2020. Copper-doped ZIF-8 with high adsorption performance for removal of tetracycline from aqueous solution. J. Solid State Chem. 285, 121219.
Sun, X., Zheng, Z., Ma, J., Xian, T., Liu, G., Yang, H., 2024. Development of ternary Pt/$BaTiO_3$/Bi_2O_3 heterostructured piezo-photocatalysts for antibiotic degradation. Appl. Surf. Sci. 653, 159421.
Tang, Y., Tai, R., Song, X., Gao, S., Wu, R., Chen, S., Li, P., Wang, Q., 2024. Zinc-Doped BiOBr Hollow Microspheres for Enhanced Visible Light Photocatalytic Degradation of Antibiotic Residues. Langmuir 40, 6515–6523.
Truong, H.B., Huy, B.T., Lee, Y.I., Nguyen, H.T., Cho, J., Hur, J., 2023. Magnetic visible-light activated photocatalyst $CuFe_2O_4$/Bi_2WO_6/mpg-C_3N_4 for the treatment of natural organic matter. J. Chem. Eng. 453, 139777.
Urakami, N., Kensuke, T., Masahiro, S., Yoshio, H., 2023. Thermal chemical vapor deposition of layered carbon nitride films under a hydrogen gas atmosphere. Cryst. Eng. Comm. 25, 877–883.
Wang, Z., Lai, C., Qin, L., Fu, Y., He, J., Huang, D., Li, B., Zhang, M., Liu, S., Li, L., Zhang, W., Yi, H., Liu, X., Zhou, X., 2020. ZIF-8-modified $MnFe_2O_4$ with high crystallinity and superior photo-Fenton catalytic activity by Zn-O-Fe structure for TC degradation. J. Chem. Eng. 392, 124851.
Wang, S., Long, J., Jiang, T., Shao, L., Li, D., Xie, X., Xu, F., 2021. F, Magnetic Fe_3O_4/CeO_2/g-C_3N_4 composites with a visible-light response as a high efficiency Fenton photocatalyst to synergistically degrade tetracycline. Sep. Purif. Technol. 278, 119609.
Wei, Z., Liu, J., Shangguan, W., 2020. A review on photocatalysis in antibiotic wastewater: Pollutant degradation and hydrogen production. Chin. J. Catal. 41 (10), 1440–1450.
Wu, F.D., Chen, J.C., Hu, J.P., 2022. Synthesis of TiO_2/$Ti_3C_2T_x$/AgI Z-scheme photocatalyst for tetracycline hydrochloride photocatalytic degradation. J. Environ. Chem. Eng. 10, 107117.
Wu, C., Dai, J., Ma, J., Zhang, T., Qiang, L., Xue, J., 2023. Mechanistic study of B-TiO_2/$BiVO_4$ S-scheme heterojunction photocatalyst for tetracycline hydrochloride removal and H2 production. Sep. Purif. Technol. 312, 123398.
Wu, C.J., Maggay, I.V., Chiang, C.H., Chen, W., Chang, Y., Hu, C., Venault, A., 2023. Removal of tetracycline by a photocatalytic membrane reactor with MIL-53 (Fe)/PVDF mixed-matrix membrane. Chem. Eng. J. 451, 138990.
Xia, K., Li, Z., Zhou, X., 2019. Ultrasensitive detection of a variety of analytical targets based on a functionalized low-resistance AuNPs/β-Ni (OH) 2 nanosheets/Ni foam sensing platform. Adv. Funct. Mater. 29 (39), 1904922.
Xie, J., Luo, X., Chen, L., Gong, X., Zhang, L., Tian, J., 2022. ZIF-8 derived boron, nitrogen co-doped porous carbon as metal-free peroxymonosulfate activator for tetracycline hydrochloride degradation: Performance, mechanism and biotoxicity. J. Chem. Eng. 440, 135760.
Yuan, J., Zhou, H., Li, D., Xu, F., 2023. F, Construction of Fe_3S_4/g-C_3N_4 composites as photo-Fenton-like catalysts to realize high-efficiency degradation of pollutants. Ceram. Int. 49, 16070–16079.
Yue, L., Zeng, Z., Ren, X., Yuan, S., Xia, C., Hu, X., Zhao, L., Zhuang, L., He, Y., 2024. Synthesis of Efficient S-Scheme Heterostructures Composed of $BiPO_4$ and $KNbO_3$ for Photocatalytic N_2 Fixation and Water Purification. Langmuir 40, 4953–4965.
Zhang, B., He, X., Yu, C., Liu, G., Ma, D., Cui, C., Yan, Q., Zhang, Y., Zhang, G., Ma, J., Xin, Y., 2022. Degradation of tetracycline hydrochloride by ultrafine TiO_2 nanoparticles modified g-C_3N_4 heterojunction photocatalyst: Influencing factors, products and mechanism insight. Chin. Chem. Lett. 33, 1337–1342.
Zhao, C., Li, X., Yue, L., Yuan, S., Ren, X., Zeng, Z., Hu, X., Wu, Y., He, Y., 2023. One-step preparation of novel Bi-Bi_2O_3/$CdWO_4$ Z-scheme heterojunctions with enhanced performance in photocatalytic NH_3 synthesis. J. Alloys Compd. 968, 171956.
Zhao, C., Li, X., Yue, L., Ren, X., Yuan, S., Zeng, Z., Hu, X., Wu, Y., He, Y., 2023. Y, Bi_4O_5Br 2 nanoflower and CdW_O4 nanorod heterojunctions for photocatalytic synthesis of ammonia. ACS Appl. Nano Mater. 6, 15709–15720.
Zhao, C., Li, X., Yue, L., Ren, X., Yuan, S., Zeng, Z., He, Y., 2023. Fabrication of novel $BiPO_4$/Bi_4O_5Br 2 heterojunctions for improving photoactivity in $_N$2 fixation and dye degradation. Mater. Res. Bull. 167, 112377.
Zhou, P., Chen, F., Su, X., Zhang, T., Meng, S., Xie, M., Song, Y., Yan, X., 2023. Ag_2O modified magnetic $BaFe_{12}O_{19}$/C_3N_4 photocatalysts with enhanced antibiotic removal: Photocatalytic mechanism and toxicity evaluation. Adv. Powder Technol. 34, 104015.
Zhou, Y., Feng, S., Duan, X., Wu, W., Ye, Z., Dai, X., Wang, Y., Cao, X., 2022. Stable self-assembly Cu_2O/ZIF-8 heterojunction as efficient visible light responsive photocatalyst for tetracycline degradation and mechanism insight. J. Solid State Chem. 305, 122628.
Zhou, H., Wang, S., Jiang, J., Shao, L., Li, D., Yuan, J., Xu, F., 2022. F, Magnetic Fe_3S_4/MoS_2 with visible-light response as an efficient photo-Fenton-like catalyst: Validation in degrading tetracycline hydrochloride under mild pH conditions. J. Alloys Compd. 921, 166023.